Journal of Solid State Chemistry **150,** 250–257 (2000)
doi:10.1006/jssc.1999.8562, available online at http://www.idealibrary.com on IDEAL®

Synthesis, Structure, and Physical Studies of the New β-$LiVOAsO_4$ Compound

J. Gaubicher,*,[1] F. Orsini,† T. Le Mercier,* S. Llorente,* A. Villesuzanne,‡ J. Angenault,* and M. Quarton*

*Laboratoire de Cristallochimie du Solide, Université Pierre et Marie Curie-Paris VI, 4 place Jussieu, 75252 Paris Cedex 05, France;
†Laboratoire de Réactivité et de Chimie du Solide, Université Jules Verne, 33 rue St-Leu, 80039 Amiens Cedex, France; and
‡Institut de Chimie de la Matiére Condensée, Université Bordeaux I, 162 Av. du Dr. A. Schweitzer, 33608 Pessac Cedex, France

Received July 12, 1999; in revised form October 20, 1999; accepted November 5, 1999

Two new compounds of the A_xMOXO_4 family, β-$LiVOAsO_4$ and β-$VOAsO_4$, have been synthesized by solid state reaction and electrochemical lithium deintercalation from β-$LiVOAsO_4$, respectively. Both compounds are isostructural and are built like other β-$VOXO_4$ (X = S, P) by $(VO_5)_\infty$ chains of distorted VO_6 octahedra connected via corner-shared AsO_4 tetrahedra. For β-$LiVOAsO_4$ the additional Li^+ ions occupy chains of edge-shared octahedra running perpendicularly to the $(VO_5)_\infty$ chains. The one-dimensional antiferromagnetic behavior suggested by the structure has been experimentaly confirmed. It is shown that lithium deintercalation occurs through a first-order transition at 4.02 V vs Li^+/Li^0. From chemical bond considerations it is shown why the redox potential of a given transition element M in a six-fold coordination involving $(M=O)^{m+}$ units lies between those observed in oxides and in $M_2(XO_4)_3$ compounds with $(XO_4)^{n-}$ oxo anions (X = S, P, As).

***Key Words*: synthesis and structure of β-$LiVOAsO_4$; magnetic behavior; lithium intercalation.**

INTRODUCTION

Compounds of the general formula $A_xMOXO_4 \cdot nH_2O$ (A = Li, Na, K; M = Ti, V, Nb, Mo; X = P, S, As; $0 \le n \le 2$) have attracted considerable attention over the past 30 years. Among these compounds, Nb and V phosphates (or arsenates) constitute an important class of materials that have been intensively studied by numerous structural and spectroscopic methods, as a result of Hein potential use in catalitic oxidation reactions and other industrial applications.

Two allotropic forms of $NbOPO_4$ are known: the tetragonal α phase is stable at low temperature (1) and the β form prepared at high temperature is monoclinic (5). In the case of the vanadyl compounds, two polymorphs are also encountered: the α form, known to be tetragonal (1), and the β, form, known to be orthorhombic (6). The former is a lamellar compound characterized by a strong anisotropy of its chemical bonds, whereas the β form exhibits a three-dimensional structure with interconnected channels. For industrial application purposes, β-$VOPO_4$ evoked a great deal of interest in the oxidation catalysis field (7). In addition, many studies have been allocated to topotactic chemical intercalation of various guest species, especially in the hydrates $MOXO_4 \cdot nH_2O$. This soft chemistry route gives rise to the $A_xMOXO_4 \cdot nH_2O$ compounds (A = Li, Na, or an organic molecule) (8).

Recently, we investigated the electrochemical and structural behaviors of the Li/β-$VOSO_4$ (9) and Li/β-$VOPO_4$ (10) systems; these compounds present interesting electrochemical behaviors. We showed that the Li/β-$VOSO_4$ system exhibits a very good reversibility during the lithium intercalation–deintercalation process after the first cycle. Concerning Li/β-$VOPO_4$, owing to a formation process of the material-to-lithium intercalation, the capacity increases on cycling. To restrain this formation process to the first oxidation, the isotypic β-$Li_{0.92}VOPO_4$ compound was synthesized. The Li/$Li_{0.92}VOPO_4$ system appears attractive since the capacity retention is excellent with a constant working voltage close to 3.95 V (355 (W h)/kg).

To complete these studies, the synthesis of β-$LiVOAsO_4$ was undertaken. The present work is concerned with its structural characterization along with its magnetic and electrochemical properties. We will also consider the contribution of the inductive effect to the redox energy of the V^{5+}/V^{4+} redox couple.

EXPERIMENTAL

The new phase, β-$LiVOAsO_4$, was obtained by reacting $VOAsO_4 \cdot 2H_2O$ with Li_2CO_3 in the molar ratio 2 : 1. The

[1] To whom correspondence should be adressed. Departement of Chemistry, University of Waterloo, Waterloo, Ontario N2L 3G1, Canada. Fax: 519-746-0435. E-mail: jgaubich@sciborg.uwaterloo.ca.

0022-4596/00 $35.00

mixture was first heated at 300°C for half an hour, and then the temperature was gradually increased (150°C/h) to 600°C and held at this temperature overnight under a constant argon flow. It is worth noting that the reagent $VOAsO_4 \cdot 2H_2O$ used in this study was obtained after 24 h, owing to the low stability of $VOAsO_4 \cdot 3H_2O$ which exhibits a loss of water at ambient temperature. $VOAsO_4 \cdot 3H_2O$ was carefully prepared according to Chernorukov's procedure (11) with the aim to minimize V^{4+} defects known to be present in this compound. Thus, V_2O_5 was refluxed in a solution of $H_3AsO_4 \cdot 0.5H_2O$ in 200 ml of distilled water for 3 days at 100°C with additions of small amounts of concentrated nitric acid.

DTA and DTG experiments were performed on β-LiVOAsO$_4$ using an automatic SETARAM system. The experiment was carried out under a constant argon flow with both the heating and cooling rates at 300°C/h in the temperature range from 25 to 900°C. The sample shows an endothermic peak beginning at 710°C with a 15% mass loss. Upon cooling, two exothermic peaks were observed at 480 and 460°C. The compound decomposition is then assumed to occur at 710°C, leading to a amorphous product by XRD.

X-ray diffraction patterns were recorded with an automatized Philips PW1050 goniometer using Cu$K\alpha$ radiation ($\lambda = 1.5418$ Å). Data were collected over the range $16° < 2\theta < 86°$ with a step width of 0.02° and count time of 25 s/step.

Magnetic susceptibility was measured in the temperature range 4.2–300 K with a MANICS DSM8 susceptometer. EPR experiments were performed on a Bruker-ESP 300 spectrometer operating at X-Band (9.5 GHz) frequencies.

Electrochemical intercalation studies were performed in both galvanostatic and potentiodynamic modes using a MacPile system (Bio-Logic, Claix, France) and Swagelok type cells, with Li metal as the negative electrode and 1 M $LiClO_4$ in anhydrous propylene carbonate as the electrolyte. Composite positive electrodes were made of 5 wt% of polyvinylidene fluoride (PVDF) and various amounts of acetylene black (4 N, Strem Chemicals) as the electronic binder, in suspension in cyclopentanone. The resulting mixture was casted on a stainless steel disk and then dried under vacuum at 80°C. For basic studies, performed with potentiodynamic methods, 25 wt% acetylene black was used to ensure complete electronic contact between every grain of the active material; for galvanostatic cycling experiments, only 15 wt% was used.

The band structure of β-LiVOAsO$_4$ was computed using the Extended Hückel tight-binding (EHTB) method (12–16), with the program EHMACC (Quantum Chemistry Program Exchange n°571). The full crystal structure of β-LiVOAsO$_4$ was used as input for the calculations. EHTB parameters are listed in Table 1. The EHTB method, not of the self-consistent field type, gives qualitative information on energetic quantities as band widths or band gaps; on the other side, it allows quantitative studies on chemical bonding and on the relations between crystalline and electronic structures (17–20). In particular, the crystal orbital overlap populations (COOP) give the bonding or antibonding contribution of energy bands toward selected bonds in the crystal. This method was used here to investigate the nature of bands around the Fermi level and their splitting due to the distribution of bond lengths.

TABLE 1
Atomic Coordinates Obtained from the Rietveld Refinement of β-LiVOAsO$_4$

Atom	Wyckoff position	x/a	y/b	z/c	B_{iso} (Å^2)
Li	4*a*	0	0	0	2.73(7)
V	4*c*	0.326(2)	$\frac{3}{4}$	0.225(2)	0.08(4)
As	4*c*	0.376(1)	$\frac{1}{4}$	0.128(2)	0.08(4)
O(1)	4*c*	0.119(7)	$\frac{3}{4}$	0.165(7)	0.47(9)
O(2)	4*c*	0.816(8)	$\frac{3}{4}$	−0.003(8)	0.47(9)
O(3)	4*c*	0.066(8)	$\frac{1}{4}$	0.495(7)	0.47(9)
O(4)	8*d*	0.872(5)	0.455(7)	0.235(5)	0.47(9)

CRYSTAL STRUCTURE

The crystal structure of β-LiVOAsO$_4$ was refined by the Rietveld method using the FULLPROF program (21). A comparison of X-ray powder diffraction data with inorganic compounds of the ICDD data bank evidenced close similarities with $LiTiAsO_5$ (JCPDS no. 44-0082) which crystallizes in the orthorhombic system, space group *Pnma*, and $Z = 4$. The structure parameters of $LiTiAsO_5$ (22) were then used as the starting model for a Rietveld refinement.

At first, a full pattern matching was performed: 8 profile parameters were allowed to refine including 2θ zero point and the unit cell parameters. This gave an excellent fit to the data. Then, after all the atomic positions led to convergence, the isotropic thermal vibration parameters were refined giving satisfactory results. In total, 25 parameters were refined for 135 independent reflections. The final reliability factors were $R_{wp} = 5.4\%$, $R_B = 4.1\%$, $R_F = 4.6\%$, and $\chi^2 = 4.1$. The corresponding X-ray powder diffraction patterns are given in Fig. 1. The unit cell parameters refined values are $a = 7.5916(2)$ Å, $b = 6.4713(2)$ Å and $c = 7.4216(2)$ Å. The final atomic coordinates are given in Table 1; the bond lengths and angles are listed in Table 2.

To check the validity of the β-LiVOAsO$_4$ structure, bond strength sums (denoted S_i) were calculated using the Brown model (23). $S_i = \sum_j (R_{ij}/R_1)^{-N}$, where R_{ij}, R_1, and N are equal to 1.378 Å and 4.065 for Li^+, 1.77 Å and 5.2 for V^{4+}, and 1.746 Å and 6.05 for As^{5+}. According to this model, V_i, the formal oxidation state of the involved i cation, is generally equal to S_i within a 5% error. The corresponding

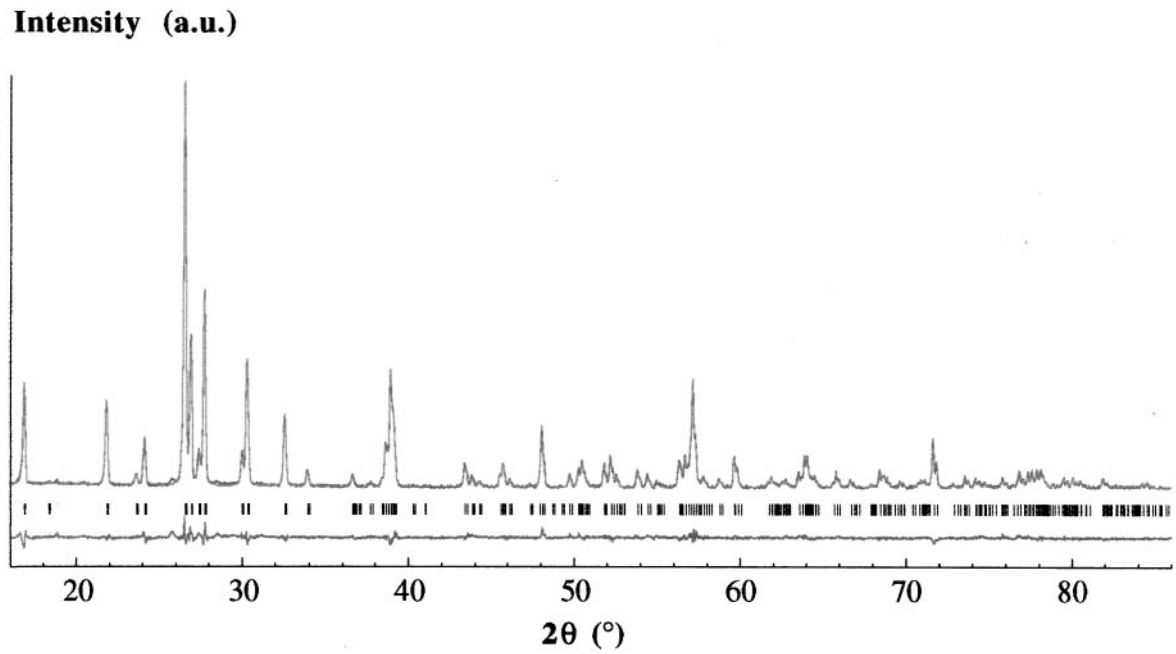

FIG. 1. X-ray diffraction profiles of the experimental and calculated patterns. The difference plot has been reported below, on the same scale.

calculations give 1.05 for Li^{+}, 4.14 for V^{4+}, and 4.86 for As^{5+}. Such results show a good chemical connection with respect to the principle to local charge balance.

The structural framework of β-$LiVOAsO_4$ appears very close to the other β-$VOXO_4$ compounds (X = S, P), but with inserted Li cations. In this way the structure consists of infinite chains of trans-corner-sharing VO_6 octahedra along the a axis (Fig. 2). As characterized by the whole series of the $MOXO_4 \cdot nH_2O$ compounds, the transition metal octahedron distorted as V^{4+} is cooperatively displaced from the center of the octahedron to form one very short bond V–O(1) = 1.629(6) Å. The distortion may be estimated by the parameter $\Delta = \sum_i((R_i - R_m)/R_m)^2/6$, where R_i corresponds to an individual bong length and R_m to an average one (24). The calculation gives $\Delta = 1.24 \times 10^{-2}$ which is smaller than the value found for β-$VOPO_4$ (6) (2.54×10^{-2}) but nearly the same as the one determined for α-$VOSO_4$

TABLE 2
Bond Lengths (Å) and Angles (°) in the β-$LiVOAsO_4$ Structure

V	O(1)	O(1)	O(2)	O(3)	O(4)	O(4)
O(1)	**1.629(6)**	3.988(6)	2.919(5)	2.697(5)	2.802(4)	2.802(4)
O(1)	175.7(9)	**2.371(6)**	2.617(4)	2.892(5)	2.723(5)	2.723(5)
O(2)	103.8(5)	71.9(3)	**2.066(6)**	3.876(6)	2.633(4)	2.633(4)
O(3)	99.7(5)	84.6(3)	156.5(2)	**1.893(6)**	2.803(5)	2.803(5)
O(4)	102.3(4)	77.3(2)	81.7(3)	93.4(3)	**1.958(5)**	3.868(6)
O(4)	77.3(2)	102.3(4)	81.7(3)	93.4(3)	152.9(1)	**1.958(5)**
Li	O(1)	O(1)	O(2)	O(2)	O(4)	O(4)
O(1)	**2.224(4)**	4.448(5)	2.617(4)	3.486(6)	2.723(4)	3.258(5)
O(1)	180.0(3)	**2.224(4)**	3.486(6)	2.617(4)	3.258(5)	2.723(4)
O(2)	73.8(3)	106.2(2)	**2.134(4)**	4.268(4)	3.212(7)	2.633(3)
O(2)	106.2(2)	73.8(3)	180.0(2)	**2.134(4)**	2.633(3)	3.212(7)
O(4)	79.7(2)	100.2(9)	101.3(3)	78.7(2)	**2.018(4)**	4.035(5)
O(4)	100.2(9)	79.7(2)	78.7(2)	101.3(3)	180.0(2)	**2.018(4)**
As	O(2)		O(3)	O(4)	O(4)	
O(2)	**1.734(6)**		2.911(6)	2.756(4)	2.756(4)	
O(3)	115.6(7)		**1.707(6)**	2.768(5)	2.768(5)	
O(4)	107.9(5)		109.9(5)	**1.675(4)**	2.663(6)	
O(4)	107.9(5)		109.9(5)	105.3(4)	**1.675(4)**	

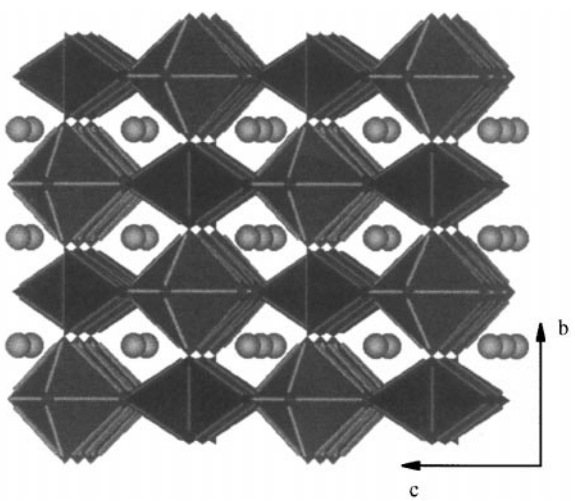

FIG. 2. Perspective view of the structure of β-$LiVOAsO_4$.

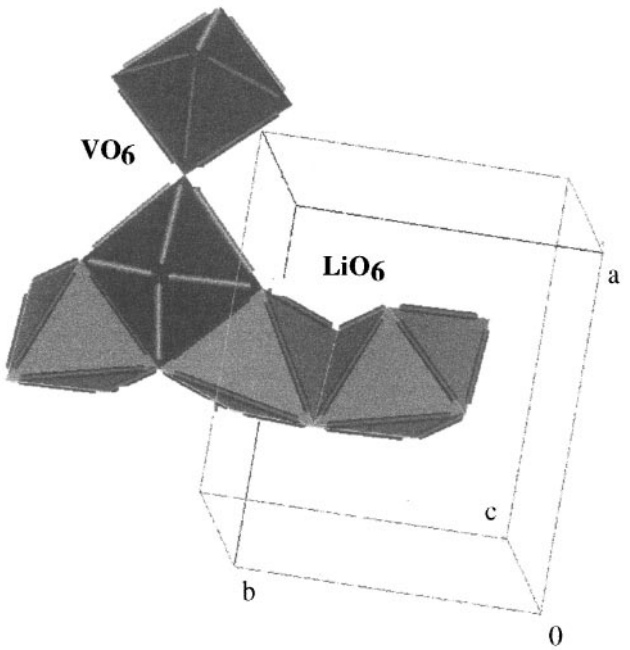

FIG. 3. Part of the $LiVOAsO_4$ structure showing the $[LiO_4]_\infty$ chains of edge-sharing LiO_6 octahedra which are face connected with VO_6 octahedra of perpendicular $[VO_5]_\infty$ chains.

(1.41×10^{-2}) (25) or β-$VOSO_4$ (1.03×10^{-2}) (26), reflecting the higher stability of V^{4+} cations in this sixfold oxygenated environment as compared with the rather small V^{5+} ions.

Two successive VO_6 octahedra of the same $(VO_5)_\infty$ chain are connected by an arsenate group causing them to be alternatively tilted with successive bond angles at the shared O(1) atoms of 60.12° and 123.42°. The two remaining corners of each given AsO_4 tetrahedron are connected to two other $(VO_5)_\infty$ chains. This arrangement between the MO_6 octahedra and the XO_4 tetrahedral groups is precisely the structural feature which causes the framework of the so called β-form to be three dimensional. On the contrary, in the α-form each corner of the tetrahedral group is linked to a different $(MO_5)_\infty$ chain in such a way that two successive octahedra are not "reticulated" by a XO_4 structural unit. Accordingly the typical long (and hence weak) M–O bond in these $(MO_5)_\infty$ chains required the α-form to be regarded as a layered structure.

The Li atom is found to be octahedrally coordinated. The LiO_6 polyhedra are connected via opposite edges to form chains along the b axis (Fig. 3). The average Li–O bond length, 2.13 Å, is consistent with the sum of the ionic radii (2.14 Å) (24). Each octahedron shares two apical corners with two AsO_4 tetrahedra and two faces with two VO_6 groups. As the distance between two successive lithium ions is the shortest along b direction (3.246 Å), when a ionic conduction mechanism occurs, lithium cations should jump cooperatively from one site to the other in this direction, through faces of the octahedra. Then it is worth noting that the corresponding windows of oxygen anion should not allow a fast ionic conductivity. In fact, taking 1.38 Å as the oxygen anion radius, the empty space in the middle of the faces consists in a circle the radius of which (0.42 Å) is smaller than the space required for a fast lithium conductivity.

MAGNETIC BEHAVIOR

As observed in Fig. 4, β-$LiVOAsO_4$ presents Curie paramagnetic behavior above 45 K. The molar Curie constant, C_M, and the paramagnetic Curie temperature, Θ_p, are determined from the equation $\chi_M = C_M/(T - \Theta_p)$ to $C_M = 0.420(3)\,cm^3\,K/mol$ and $\Theta_p = -58(1)\,K$, respectively. In agreement with the orbital contribution of a d^1 electronic configuration ($L \neq 0$) to the effective magnetic moment, the value of μ_{eff} (1.84) is different from the spin only value (1.73). χ_M first increases rapidly with decreasing temperature, reaches a maximum value at a temperature close to 30 K, and finally decreases.

Field studies at 4 K do not evidence the nonlinear effect of saturation characteristic of ferro-ferrimagnetic behavior which could be present at low temperature. Under this condition the observed behavior below 30 K would be in accordance with an antiferromagnetic ordering of the d^1 paramagnetic centers consistent with the negative sign of the paramagnetic Curie temperature. On the basis of an isotropic exchange coupling within a infinite chain, the magnetic susceptibility of a d^1 ion in antiferromagnetic chains is given by Bonner and Fisher (27),

$$\chi_M = \frac{Ng^2\mu_B^2}{kT}(0.25 + 0.14995x + 0.30094x^2) \times (1 + 1.9862x + 0.68854x^2 + 6.0626x^3)^{-1} + \frac{C_i}{T},$$

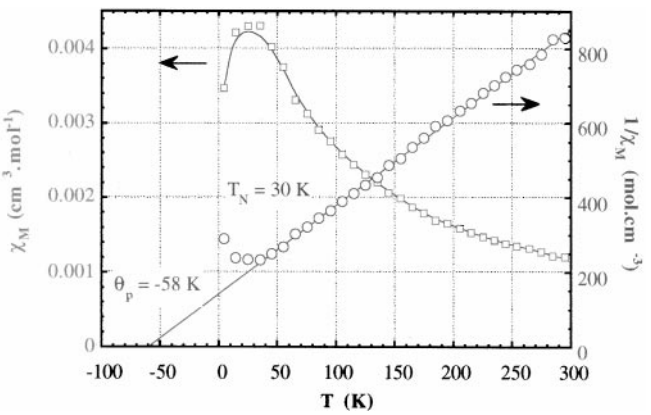

FIG. 4. Thermal dependence of the molar magnetic susceptibility (χ_M) measured for β-$LiVOAsO_4$ and its inverse $1/(\chi_M)$. The smooth curve represents a fit to the data from the Bonner and Fischer linear-chain model (27).

TABLE 3
Distances and Angles Relative to the Superexchange Magnetic Interactions Occurring for β-$LiVOAsO_4$ and β-$LiVOPO_4$

	β-$LiVOAsO_4$	β-$LiVOPO_4$
V=O (Å)	1.629(6)	1.628(3)
V···O (Å)	2.371(6)	2.342(3)
V–O–V (°)	144.2	140.7

where $x = |J|/kT$ and C_i/T is an added factor to take into account possible contribution from paramagnetic impurities. An excellent fit of the previous equation to the whole data (Fig. 4) was obtained for physically reasonable values of the exchange constant $J = -16.8(3)\,cm^{-1}$ and the Landé factor $g = 1.96(2)$. C_i was refined to 0.0012(6) cm^3 K/mol which confirms the very good magnetic purity of our compound since the corresponding amount of isolated paramagnetic V^{4+} defects is calculated to 0.3%. The validity of the g value was checked by EPR experiments of this material at 77 K and 298 K ($g = 1.957$).

These values are extremely close to the one found by Lii *et al.* for the isostructural β-$LiVOPO_4$ compound (28): $J = -22\,cm^{-1}$, $g = 1.96(2)$, and $C_i = 0.0057\,cm^3$ K/mol. In the same way, they found $C = 0.4168\,cm^3$ K/mol, $\Theta_p = -67.5$ K, and $T_N = 40$ K. Assuming that the magnetic exchanges consist in superexchange interactions via the apical oxygen atoms O(1) further more strictly confined to the $(VO_5)_\infty$ chains, one expects the V–O(1) bonds along the chain direction and the corresponding V–O(1)–V angles to be nearly the same for the two isotypic compounds. Such values, gathered in Table 3, confirm this assumption. In order to correlate the geometric characteristics of the $(VO_5)_\infty$ chains and the magnetic behavior one can use the Kamamori–Goodenough rules (29). The band structure calculation obtained for β-$LiVOAsO_4$ shows that the V^{4+} d^* levels located between -11 and -5 eV are nondegenerated (Fig. 5). The fundamental level at -10 eV is a half filled singlet orbital. Under this condition, either delocalization or correlation superexchange mechanism results in antiparallel couplings leading to the experimentally observed macroscopic antiferromagnetism.

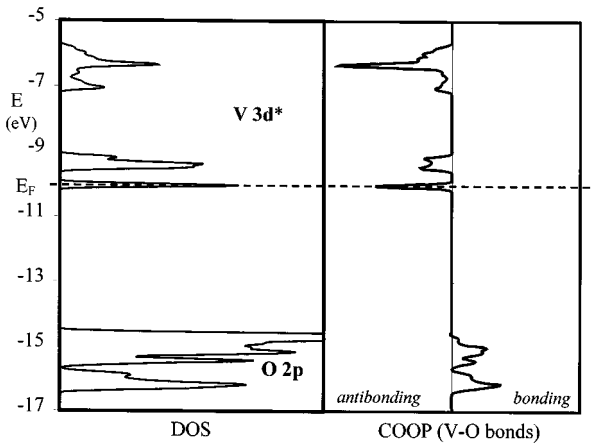

FIG. 5. Density of states (DOS) and vanadium–oxygen overlap population (COOP V–O bonds) for $LiVOAsO_4$, calculated with the EHTB method.

ELECTROCHEMICAL BEHAVIOR

Our previous works concerning Li/β-$VOSO_4$ (9) and Li/β-$VOPO_4$ (10) systems indicate that these compounds are suitable for the lithium intercalation to occur. For Li/β-$LiVOAsO_4$ the redox process pertaining to the V^{5+}/V^{4+} couple implies that the lithium is first removed and then reintercalated in the host. Figure 6 shows a typical incremental capacity voltammogram, obtained for the first cycles from a stepwise potentiodynamic cycling with ± 10 mV steps every 1.5 h within a 3.3–4.2 V potential window. It appears that after a specific behavior on first oxidation, the redox process occurs in one step denoted "R/O". The relative positions of the incremental capacity peaks are clearly characteristic of a two-phase process. The intercept of the initial slope with the abscissae at 4.02 V on oxidation corresponds to the equilibrium two-phase potential.

This result is supported by the traces of the chronoamperometric responses to the potential steps: in Fig. 7, for the first reduction (R_1 step) the reduction current increases slightly when stepping from 4.02 to 4.01 V and very significantly at the next step. Simultaneously, the time dependence of the current during these potential levels departs from a diffusion-controlled process (Fick's law). This is the signature of crossing the characteristic potential of a two-phase equilibrium just above 4.01 V. Moreover, such a shape of the chronoamperograms is typical of a redox process with a phase transformation where the limiting factor of the kinetics is the phase transformation (30).

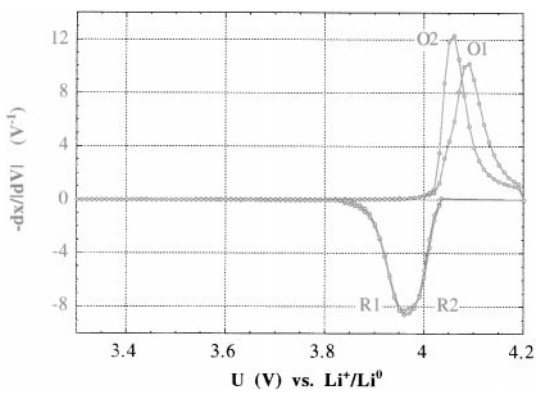

FIG. 6. Incremental capacity voltammogram obtained for β-$LiVOAsO_4$ from a stepwise potentiodynamic cycling with ± 10 mV steps every 1.5 h.

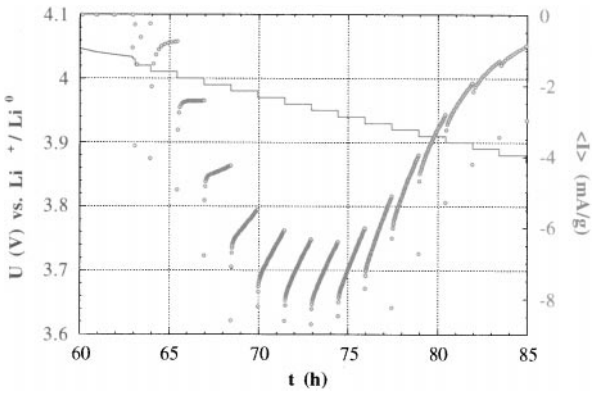

FIG. 7. Chronoamperograms of the first reduction (R_1 step) showing the specific behavior of the current when crossing the two-phase equilibrium at about 4.02 V.

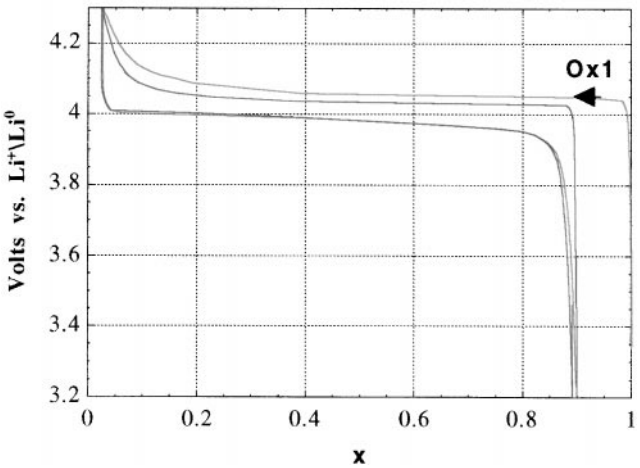

FIG. 8. Potential–composition curve obtained after the two first cycles for β-LiVOAsO$_4$ upon galvanostatic cycling at nominal C/50 regime (0.013 mA/cm^2; 2.584 mA/g).

The first oxidation peak (O1) is significantly broader than the second one, along with a smaller initial slope. The kinetics of the first oxidation is thus slower than that of the second. This phenomenon suggests a formation process occuring within the material that might be related to the creation of structural defects associated with the first lithium deintercalation. As evidenced by the similarity of the R_1 and R_2 reduction peaks, the kinetics of the reduction processes is constant. This result confirms what has been inferred by the Li/β-VOPO$_4$ study (10): the direct synthesis of lithiated compounds β-Li$_x$VOXO$_4$ acts to restrain formation processes to the first oxidation. In addition, like the oxides LiMn$_2$O$_4$, LiCoO$_2$, and LiNiO$_2$, direct synthesis avoids reactions with ambient atmosphere which are encountered with V$^{\text{V}}$OXO$_4$ compounds.

The galvanostatic cycling behavior is reported in Fig. 8 for the first two cycles at a C/50 regime (0.013 mA/cm^2; 2.584 mA/g) within a 3.2- to 4.3-V potential window. As inferred by the voltammetry, the kinetics during the first oxidation process is the slowest: the polarization decreases from 90 mV upon the first cycle to 70 mV. The kinetics of this system is faster than the one observed for the analogous Li/β-Li$_{0.92}$VOPO$_4$ system for which the polarization is slightly higher than 80 mV upon cycling (in the same experimental conditions) (10). In addition, the efficiency is higher for the arsenate compound since it maintains at 87% of the theoretical capacity after a 10% loss upon the first cycle, compared to 55% for β-Li$_{0.92}$VOPO$_4$. We believe this difference to be the result of pyrophosphate groups that might be formed when synthesizing the β-VOPO$_4$ precursor (10) (^{31}P NMR experiments are in progress to address this issue). These groups would hinder the intercalation–deintercalation kinetics. In Fig. 9, a very good cyclability is observed at least for the 22 first cycles since the specific capacity remains higher than 105 (mA h)/g at a constant potential of 4 V, that is, 420 (W h)/kg.

To determine the structural evolution of β-LiVOAsO$_4$ upon lithium deintercalation–intercalation, ex situ XRD patterns were recorded at different redox levels after potentiostatic equilibration: at 4.20 V until the current had reached a value equivalent to a C/1000 regime for completion of the first oxidation step, and after $x = 0.15$ on the following reduction. The corresponding diffractograms are reported in Fig. 10.

Pattern b has been obtained upon first oxidation after the deintercalation of one Li. The appearance of new diffraction lines indicates the formation of a new phase of formula VOAsO$_4$. It presents a diffractogramm different from the one corresponding to the unique vanadyl arsenate compound reported in the litterature, that is, α-VOAsO$_4$ (JCPDS 33-1446).

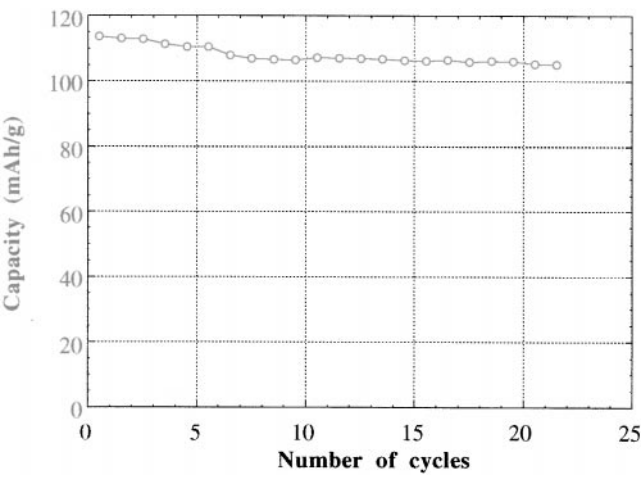

FIG. 9. Capacity retention of β-LiVOAsO$_4$ on cycling at C/50 regime (0.013 mA/cm^2; 2.584 mA/g).

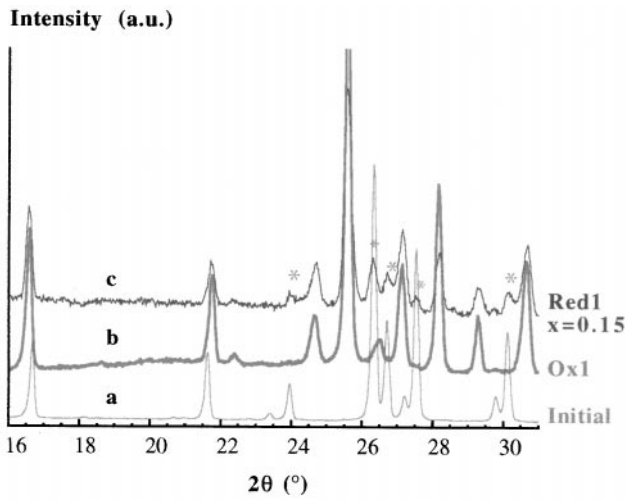

FIG. 10. Ex situ X-ray diffraction patterns of β-Li_xVOAsO_4 at various redox levels: (a) pristine β-$LiVOAsO_4$; (b) after completion of the first oxidation process; (c) on the first reduction step R_1 at $x = 0.15$.

Pattern c shows that upon the following reduction at $x = 0.15$ the pristine β-$LiVOAsO_4$ is restored (new peaks labeled *). The coexistence of the two phases confirms that the redox process is a first-order transition.

Noting that the crystal structures of β-$Li_{0.92}VOPO_4$ (obtained after lithium intercalation in β-$VOPO_4$) and β-$LiVOAsO_4$ are closely related (10), and assuming that the structural behaviors of these compounds upon lithium deintercalation are similar, we expected the variation of the unit-cell parameters to be the same for both cases. In this way the parameters of $VOAsO_4$ were refined by a full pattern matching method (21) with space group *Pnma*. The obtained values are reported in Table 4 along with the goodness of fit χ^2. The new crystalline form of $VOAsO_4$, isostructural with the pristine β-$LiVOAsO_4$ compound, has been labeled β-$VOAsO_4$.

Recently, Goodenough *et al.* investigated new Nasicon type electrode materials with the general formula $Li_xM_2(XO_4)_3$ (M = transition metal; X = S, P, As) (31, 32). They were able to separate the contibution of the structure from that of the covalency of the metal–oxygen bond on the potential level of the redox couples: the more ionic the M–O bond, the lower the energy of the antibonding d orbitals and the higher the potential of the redox couple. Accordingly, by analogy to the spectroscopic series, an "electrochemical series" can be established in which the redox potential of a given $M^{n+}/M^{(n+1)+}$ couple varies as follows:

$$E^\circ(O^{2-}) < E^\circ(PO_4^{3-}) \approx E^\circ(AsO_4^{3-}) < E^\circ(SO_4^{2-}).$$

Herein, we assume that the isostructural β-Li_xVOXO_4 compounds (X = S, P) have a band structure similar to that established for β-$LiVOAsO_4$. In this condition, it should be pointed out that the d electron acceptor level has an antibonding character (Fig. 5) and thus that the redox energy partly depends on the nature of the X atom via the inductive effect.

For β-$LiVOAsO_4$ the V^{5+}/V^{4+} redox couple lies at 4.02 V vs Li^+/Li^0. Such a potential is comparable to that found for the analogous Li/β-$VOPO_4$ system, as expected from the fact that As–O and P–O bonds present nearly the same covalency (which implies a similar contribution of the inductive effect). This is in accordance with the report by Masquelier *et al.* who established that the Fe^{3+}/Fe^{2+} redox couple lies close to 2.8 V for both $Li_3Fe_2(XO_4)_3$ (X = P, As) (31).

The comparison of the 4.02-V value obtained for V^{5+}/V^{4+} to that found for oxides and Nasicon type compounds, indicates that it is an intermediate voltage. In V_2O_5, which also contains one V=O bond per vanadium atom, the V^{5+}/V^{4+} redox couple lies close to 3.3 V. Considering the "electrochemical series," this can be qualitatively explained by taking into account that from V_2O_5 to β-$LiVOAsO_4$ the four V–O bonds are replaced by the more ionic V–O(–As) bonds. On the other hand, the V^{4+}/V^{3+} redox couple was reported to be at 3.8 V in $Li_{3-x}V_2(PO_4)_3$ by Goodenough *et al.* (32). As the high-voltage limit of their electrolyte was close to 4.5 V, they did not succeed in deintercalating more than 2 Li per formula unit. Accordingly, the V^{5+}/V^{4+} redox couple energy could not be measured in an octahedral environnment of $(PO_4)^{3-}$ units and was estimated to be higher than this experimental limit. In β-$LiVOAsO_4$, as we had previously established for β-$VOSO_4$ (9) and β-$VOPO_4$ (10), the highly covalent character of the vanadyl bond lowers the potential of the redox couple to 4.02 V vs Li^+/Li^0.

TABLE 4
Cell Parameters, Volume, and Goodness of Fit Obtained for β-$LiVOAsO_4$ and β-$VOAsO_4$

	a (Å)	b (Å)	c (Å)	$V_{f.u.}$ (Å^3)	χ^2
β-$LiVOAsO_4$	7.5916(2)	6.4713(2)	7.4216(2)	91.1(3)	4.1
β-$VOAsO_4$	7.922(2)	6.316(2)	7.194(2)	90.0(3)	6.3

CONCLUSION

The synthesis of the new β-$LiVOAsO_4$ material has been carried out via a solid state reaction. The structure of this compound has been refined in the *Pnma* space group by the Rietveld method. It is described as being very close to the β-$VOXO_4$ structural family (X = S, P), but with Li inserted into channels and constituting edge-connected LiO_6 octahedra. As predicted from the structure, the magnetic study demonstrated a one-dimensionnal antiferromagnetic

behavior, the amplitude of which has been evaluated. The electrochemical behavior study showed that the intercalation occurs via a two-phase process at 4.02 V vs Li^+/Li^0 and gives rise to an isostructural delithiated compound. From a fundamental point of view, taking into account the inductive effect contribution, it has been shown that a covalent $(M{=}O)^{n+}$ unit places the redox couple energy of a given transition element M in a six-fold coordination between that observed in corresponding oxides and in $M_2(XO_4)_3$ (X = S, P, As) compounds.

ACKNOWLEDGMENTS

The authors are grateful to Dr. Yves Chabre (Grenoble, France) and Pr. Michel Armand (Univerity of Montreal, Canada) for fruitful discussions.

REFERENCES

1. J. M. Longo and P. Kierkegaard, *Acta Chem. Scand.* **20,** 72 (1966).
2. H. A. Eick and L. Kihlborg, *Acta Chem. Scand.* **20,** 722 (1966).
3. K. Beneke and G. Lagaly, *Inorg. Chem.* **22,** 1503 (1983).
4. S. Bruque, M. Martinez Lara, L. Moreno, T. Ramirez-Cardenas, J. Chaboy, M. Marziali, and S. Stizza, *J. Solid State Chem.* **114,** 317 (1995).
5. H. Chahboun, D. Groult, M. Hervieu, and B. Raveau, *J. Solid State Chem.* **65,** 331 (1986).
6. R. Gopal and C. Calvo, *J. Solid State Chem.* **5,** 432 (1972).
7. E. Bordes and P. Courtine, *J. Catal.* **57,** 236 (1979).
8. A. J. Jacobson, J. W. Johnson, J. F. Brody, J. C. Scanlon, and J. T. Lewandowski, *Inorg. Chem.* **24,** 1782 (1985).
9. J. Gaubicher, Y. Chabre, J. Angenault, A. Lautié, and M. Quarton, *J. Alloys Compd.* **262–263,** 34 (1997).
10. J. Gaubicher, T. Le Mercier, Y. Chabre, J. Angenault, and M. Quarton, *J. Electrochem. Soc.* **146**(12), 4375–4379 (1999).
11. N. G. Chernorukov, N. P. Egorov, and I. A. Korshunov, *Russ. J. Inorg. Chem.* **23,** 10 (1978).
12. R. Hoffmann, *J. Chem. Phys.* **39,** 1397 (1963).
13. J. H. Ammeter, H. B. Bürgi, J. C. Thibeault, and R. Hoffmann, *J. Am. Chem. Soc.* **100,** 3686 (1978).
14. M.H. Whangbo and R. Hoffmann, *J. Am. Chem. Soc.* **100,** 6093 (1978).
15. T. Hughbanks and R. Hoffmann, *J. Am. Chem. Soc.* **105,** 3528 (1983).
16. R. Hoffmann, "Solids and Surfaces: A Chemist's View of Bonding in Extended Structures." VCH, New York, 1988.
17. E. Canadell and M. H. Whangbo, *Chem. Rev.* **91,** 965 (1991).
18. J. K. Burdett, "Chemical Bonding in Solids." Oxford University Press, New York, 1995.
19. J. K. Burdett and S. A. Gramsh, *Inorg. Chem.* **33,** 4309 (1994).
20. A. Simon, *Angew. Chem. Int. Ed. Engl.* **36,** 1788 (1997).
21. J. Rodriguez-Carjaval, "FULLPROF: Rietveld, profile matching and integrated intensity refinement of X-ray and/or neutron data, Version 3.5.d, Oct. 98," Laboratoire Léon Brilloin, CEA, Saclay, France.
22. A. Robertson, J. G. Fletcher, J. M. S. Skakle, and A. R. West, *J. Solid State Chem.* **109,** 53 (1994).
23. I. D. Brown and K. K. Wu, *Acta Crystallogr. B* **32** 1957 (1976).
24. R. D. Shannon, *Acta Crystallogr. A* **32,** 751 (1976).
25. J. M. Longo and R. J. Arnott, *J. Solid State Chem.* **1,** 394 (1970).
26. P. Kierkegaard and J. M. Longo, *Acta Chem. Scand.* **19,** 1906 (1965).
27. J. Bonner and M. E. Fisher, *Phys. Rev. A* **135,** 640 (1964).
28. K. H. Lii and C. H. Li, *J. Solid State Chem.* **95,** 352 (1991).
29. J. B. Goodenough, "Magnetism and the Chemical Bond." John Wiley, New York, 1963.
30. Y. Chabre, *in* "Chemical Physics of Intercalation." (P. Bernier *et al.*, Ed.). Plenum, New York, 1993.
31. C. Masquelier, A. K. Padhi, K. S. Nanjundaswamy, S. Okada, and J. B. Goodenough, *J. Solid State Chem.* **135,** 228 (1998).
32. K. S. Nanjundaswamy, A. K. Padhi, J. B. Goodenough, S. Okada, H. Ohtsuka, H. Arai, and J. Yamaki, *Solid State Ionics* **92,** 1 (1996).